

Article

# Amazon River Plume in the Western Tropical North Atlantic

Eugene G. Morozov <sup>1,\*</sup> , Dmitry I. Frey <sup>1,2</sup> , Pavel A. Salyuk <sup>3</sup>  and Maxim V. Budyansky <sup>3</sup> 

<sup>1</sup> Shirshov Institute of Oceanology, Russian Academy of Science, Moscow 117997, Russia; dima.frey@gmail.com

<sup>2</sup> Marine Hydrophysical Institute of RAS, Sevastopol 299011, Russia

<sup>3</sup> V.I. Il'ichev Pacific Oceanological Institute, Far Eastern Branch of the Russian Academy of Science, Vladivostok 690041, Russia; pavel.salyuk@gmail.com (P.A.S.); plaztic@poi.dvo.ru (M.V.B.)

\* Correspondence: egmorozov@mail.ru; Tel.: +7-967-133-1880

**Abstract:** Measurements of temperature, salinity, and currents in the Amazon River plume over a section in the open ocean of the western tropical North Atlantic (38°48' W) are considered. The measurements were carried out using an AML Base X CTD probe in the upper layer and a flow-through system that measures salinity, turbidity, and chlorophyll-a content in seawater while a vessel is on the way. The measurements were supplemented by velocity profiling using shipborne SADCP. Additionally, archived oceanographic data from the World Ocean Database (WOD18), data on satellite altimetry measurements (AVISO), and satellite salinity data from Aquarius and SMOS were used. It is shown that the width of the Amazon River plume is about 170–400 km and the depth of desalination is from 50 to 100 m. Surface salinity decreases compared to the background (36.1) by 0.25 in February and by more than 3.0 in September during the period of maximum development of the plume, which was determined from satellite measurements of surface salinity. Lagrangian modeling of the back-in-time advection of passive markers simulating freshwater particles was carried out. It was shown that the source of freshwater in the measurement area is discharge from the Amazon River. Amazon River freshwater covered a distance of 3300 km in 60–80 days. The estimate of freshwater transport in the plume was 0.02 Sv, which is one order of magnitude smaller than the mean river discharge.

**Keywords:** desalination of the surface layer; intra-annual plume variability; CTD casts; continuous recording; Lagrangian analysis; long-distance transport; region of freshwater influence



**Citation:** Morozov, E.G.; Frey, D.I.; Salyuk, P.A.; Budyansky, M.V.

Amazon River Plume in the Western Tropical North Atlantic. *J. Mar. Sci. Eng.* **2024**, *12*, 851. <https://doi.org/10.3390/jmse12060851>

Academic Editor: João Miguel Dias

Received: 16 April 2024

Revised: 14 May 2024

Accepted: 17 May 2024

Published: 21 May 2024



**Copyright:** © 2024 by the authors. Licensee MDPI, Basel, Switzerland. This article is an open access article distributed under the terms and conditions of the Creative Commons Attribution (CC BY) license (<https://creativecommons.org/licenses/by/4.0/>).

## 1. Introduction

The Amazon River is the largest river on our planet. Discharge from the Amazon River is estimated at 0.2 Sv (the annual mean discharge is about 209,000 m<sup>3</sup>/s) [1–3]. A plume of desalinated Amazon River water spreads across the entire tropical Atlantic. According to the results of recent studies [4], the dynamics of the Amazon River plume strongly affects the regime of the entire equatorial Atlantic Ocean [5] (at least within the square 60°–24° W and 5° S–16° N), reducing surface salinity by 3–8 PSU (depending on the distance traveled from the delta), the thickness of the upper quasi-homogeneous layer by 20–50 m, and mixing by forming a barrier even at a great distance from the river mouth (up to 4000 km and beyond) [6]. We use the practical salinity scale 1978 (PSS-78) for salinity everywhere in this text [7].

Spreading of the Amazon River plume in the tropical Atlantic is a result of several processes that control seasonal and inter-annual variations in the Amazon River discharge and oceanic processes including strong precipitation, ocean currents, winds, storms, and mixing [8–11].

The thickness of the plume along the Brazil shelf and in the offshore vicinity is typically 3–15 m; its width ranges between 80 and 200 km [12–14]. In the mid-Atlantic, the plume can be as thick as 50 m or greater [6,9].

The existence of the plume enhances the eastward transport of currents. The quantitative aspects of this influence remain poorly understood. The influence of Amazon River waters is felt far from the river mouth as an increase in surface stratification due to the desalination of the upper layer [15]. The Amazon River plume appears to contribute to atmosphere–ocean climate interaction dynamics in the western tropical North Atlantic. The flow of freshwater from the Amazon River into the ocean does not only lead to climate changes in the region. The river carries coastal sediments, nutrients, and colored and transparent dissolved organic matter (CDOM and DOM) into the ocean, which have been recorded as far as the coast of Africa [15]. Their entry leads to the development of phytoplankton cells and to an increase in the concentration of chlorophyll-a [9]. It was shown in [6] that the interaction of biota with nutrients in the plume leads to the absorption of atmospheric carbon dioxide by the waters of the river plume.

It was reported in [16] that variations in the Amazon River discharge influence the hydrological cycle, which have been observed to increase river flows during the wet season and to reduce water levels during the dry season since 2009. This phenomenon can affect the surface salinity of the tropical Atlantic. The authors propose a model to explain how the ocean, atmosphere, and the Amazon River forest interact to cause this hydrological intensification. Korosov and coauthors [17] analyzed the spread of the Amazon River plume, suggesting a synergistic tool based on an algorithm for deriving sea surface salinity from MODIS reflectance data together with sea surface salinity data from the SMOS and Aquarius satellites and the TOPAZ data assimilation system.

A nice illustration of the Amazon River plume spreading in the tropical Atlantic during the period from October 1 to 31, 2023 is shown in Figure 1 based on the satellite SMAP data (<https://smap.jpl.nasa.gov/data/> (accessed on 10 May 2024)) [18]. Salinity decreases in the upper layer occur due to desalinated water from the Amazon River. Additional freshwater can be provided by the discharge from the Orinoco River during its maximum flooding, which occurs in August, two months later than that of the Amazon River in June [9]. Generally, during most of the year, the Orinoco waters flow to the Caribbean Sea [19]; patterns of plume spread into the southern part of the Caribbean Sea are clearly seen in the satellite images in [20–22], while the freshwater transport across the Guyana Current to the east is low.

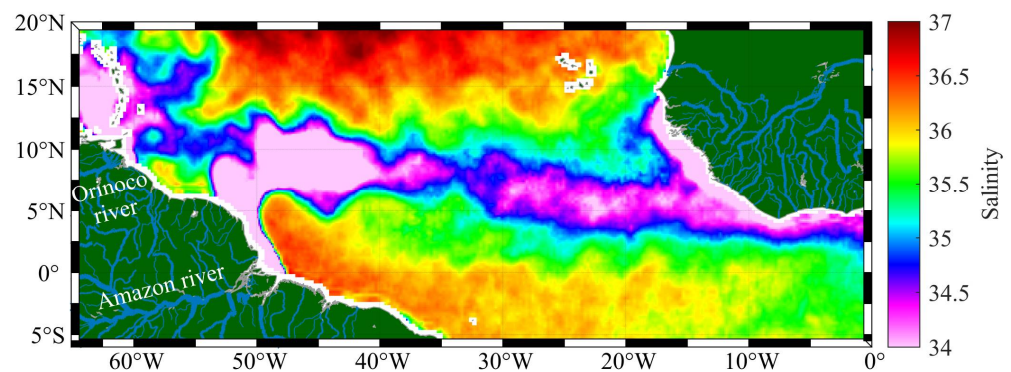


**Figure 1.** Map of monthly surface salinity based on SMAP satellite data in October 2023. (Color scale of salinity is given on the right).

Since discharge from the Amazon River occurs at the equator and in the western part of the ocean, its waters are entrained into intense currents that transport the waters further: the North Brazil Current (NBC), the North Equatorial Countercurrent (NECC), and the Guiana Current (GC) [15].

Previously, we studied the discharge from the Amazon River water to the shelf and slope region of north Brazil near the delta during an expedition in November 2022 [14]. We carried out an oceanographic survey of 30 CTD casts offshore in the Amazon River delta region. When freshwater flows out from the river, a desalination plume about 15 m thick with a sharp salinity interface is formed over the shelf. This plume is captured by

the North Brazil Current and transported first to the northwest along the South American shelf. A scheme of recirculation of the North Brazil Current and the location of quasi-stationary eddies is shown in Figure 2. The Amazon River sediment fan significantly changes the topography of the slope. This can lead to a change in the vorticity of the North Brazil Current, rotation of the current to the north and later to the east, and separation of rings [23–25]. Large rings (450 km in diameter) in the North Brazil Current separate from the mean flow and exist in the region, slowly moving to the Caribbean [21,26–28].

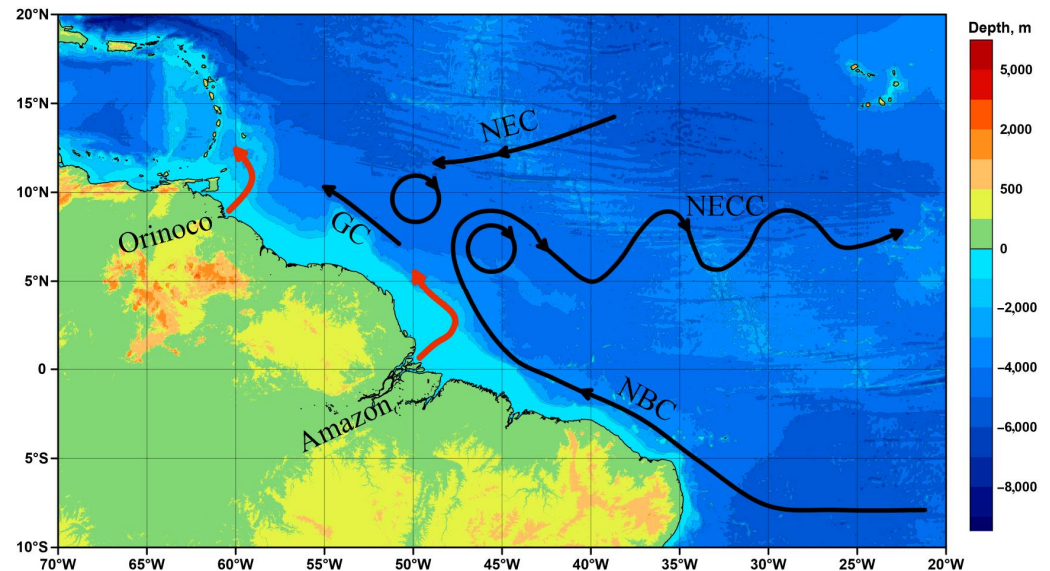


**Figure 2.** Scheme of currents in the tropical West Atlantic that transport Amazon River waters in the ocean based on [5,6,20,26,27,29–33]. Red arrows show plumes of the Orinoco and Amazon rivers. NBC is North Brazil Current; NECC is North Equatorial Countercurrent; GC is Guiana Current; and NEC is North Equatorial Current. (Color scale of depth is given on the right).

The separation of rings and rotation of the current occur approximately a hundred kilometers northwest of the Amazon River delta. A quasi-stationary meander is formed here, and the current turns east, giving rise to the North Equatorial Countercurrent. Along with the current, freshwater from the Amazon River is transported, which gradually mixes with the underlying layers and desalinizes the surface layer.

In the boreal autumn, between August and October, approximately 70% of the Amazon River plume water is captured by the NECC forming a stream of fresher waters directed to the east [6,30,34]. Seasonal variations in the intensification of the Amazon River plume were also reported in [6] based on numerical modeling supported by CTD data from the World Ocean Database. The most intense plume is usually observed in September, while lower intensities are found in January. Data on drifters also support model simulations showing the trajectories of the drifters trapped by the NECC. The estimated time of their excursion to longitude 40° W ranges from 60 to 100 days. In May–September, drifters are rapidly advected eastward by the NECC and reach 40° W–35° W after 40–60 days [6].

The studies reported in [10] were based on a survey in the region and on data of drifters and a satellite color scanner. The data confirms the trajectories of drifters transported initially by the NBC, its retroflexion, and then the NECC along low surface salinity values. This motion was observed from June to January each year. From February to May, the eastward currents weaken, and Amazon River water flows northwestward towards the Caribbean Sea.

A similar scheme of motion was reported in [35] based on numerical modeling of salinity and surface currents in the region. Limeburner et al. [36] reported about the trajectories of Amazon River water based on satellite-tracked drifters launched near the

mouth of the Amazon River. Part of the drifters first moved to the northwest and then turned to the east. One of the drifters crossed the ocean.

Mixing with surrounding waters occurs during the long-term presence of river water in sea water. Mixing is especially intense during strong winds. The Trade Winds are permanently blowing here. Thus, the thickness of the upper mixed layer increases, which leads to a significant decrease in salinity contrasts [37,38]. In addition, in the tropical and equatorial zones, the generally recognized characteristics of river waters become less pronounced in the case of a long stay of such waters in the open sea: a significant redistribution of salinity occurs due to evaporation and precipitation [39,40], and the content of colored dissolved organic matter (CDOM) decreases due to the photodestruction of molecules or changes due to the functioning of phytoplankton communities [41,42]. Therefore, the task of studying the long-distance transport of small portions of Amazon River waters is not simple.

The development of sensitive shipboard measurement methods, multi-sensor satellite sensing, and numerical methods of hydrodynamic modeling and Lagrangian analysis make it possible to study these processes at a new qualitative level, increasing the distances and time periods within which the presence of river waters in sea water can be detected.

Much of the previous analyses of the Amazon River plume spreading in the mid-Atlantic were based either on satellite data [8,9] or on numerical modeling [43–45]. Many publications are related to the Amazon River plume in the vicinity of the Amazon River delta [12,13]. Less publications analyze field measurements far from the source [6,46].

The goal of this work is to analyze the long-distance transport of Amazon River waters to the northern tropical part of the Atlantic Ocean to longitudes of 34–40° W in different seasons, as well as to develop methods for detecting small salinity contrasts and confirming their river origin. We suggest an interpretation of the Amazon River water spread in contrast to the surrounding waters. The scientific contribution of this research is in the presentation and interpretation of the collected in situ observations in the context of historical observations and studies of the Amazon River plume dynamics. With this in mind, we also applied a new approach to use shipborne SADCP measurements of currents and continuous data from the flow-through system of a ship, which makes our analysis different from previous publications. We modeled the motion of freshwater particles back in time before our measurements to show that this freshwater originates from the Amazon River delta.

## 2. Materials and Methods

On cruise 94 of the R/V Akademik Mstislav Keldysh, the vessel carried out a CTD section along the meridian 38°48.0' W from 3° N to 12° N to study currents in the equatorial and tropical zones of the Atlantic. The stations were made with a spatial step of 20 miles (in some locations, 10 miles) down to a depth of 700 m. The CTD casts were carried out with an AML Base X CTD probe. The ship crossed a plume of desalinated waters on 1–2 February 2024. The whole section was occupied on January 31–February 5. Our measurements differed from the few previous ones (those downloaded from the World Ocean Database (WOD18) were 30 miles or greater) by a higher spatial resolution of the section. The data that we used from the WOD18 were not accompanied by measurements of currents [[https://www.ncei.noaa.gov/sites/default/files/2020-04/wod\\_intro\\_0.pdf](https://www.ncei.noaa.gov/sites/default/files/2020-04/wod_intro_0.pdf)]; [<https://www.ncei.noaa.gov/products/world-ocean-database>] (accessed on 10 May 2024). The data from WOD18 were related to transoceanic sections without specific relation to the Amazon River plume spreading.

Measurements at the stations in our cruise were accompanied by continuous measurements of temperature, salinity, turbidity, and chlorophyll-a fluorescence in the vessel's flow-through system by pumping water from a depth of ~4 m through a pipe with sensors. The water properties were measured by a SeaBird SBE-45 thermosalinograph from 3° N to 12° N with a time interval of 10 s (which corresponds to a distance of ~50 m at a speed

of 10 knots) and Turner C6P optical sensor from 3° N to 7° N with a time interval of 60 s (~300 m of spatial resolution at 10 knots).

Direct velocity measurements were carried out using the onboard SADCPC: Teledyne RD Instruments Ocean Surveyor (TRDI OS) with a frequency of 76.8 kHz. We set 60 bins, each 16 m thick with an 8 m blank distance below the bottom of the ship, where the transducer was installed. This setting gives 22 m depth for the center of the uppermost layer of velocity measurements. The time averaging was 120 s. The speed of the ship was 8–10 knots; hence, measurements were made every ~500 m.

We additionally applied historical oceanographic data from the WOD18, satellite images of surface salinity from the SMOS satellite data (Soil Moisture and Ocean Salinity) [[https://www.esa.int/Applications/Observing\\_the\\_Earth/FutureEO/SMOS](https://www.esa.int/Applications/Observing_the_Earth/FutureEO/SMOS)] (accessed on 10 May 2024), and current velocities calculated from AVISO satellite altimetry data (Archiving, Validation, and Interpretation of Satellite Oceanographic Data) [<https://www.aviso.altimetry.fr/en/data/products/sea-surface-height-products/global.html>] (accessed on 10 May 2024). The altimetry data have a daily temporal resolution and spatial resolution of 0.25°. The data are available in near-real time and are updated daily.

The Lagrangian approach was used to determine the source and to model the pathways of desalinated waters to the region of measurements. Its essence is to construct a large number of marker trajectories simulating waters with specific oceanographic characteristics [47–49]. A spot (number 1) of 20,000 markers was placed on segment-1 with coordinates 5°12.0′–5°15.6′ N, 38°48′ W during the measurements on 2 February 2024, and another spot (number 2) was placed on segment-2 with coordinates 8°27′–8°33′ N, 38°48′ W on 4 February 2024. After that, based on the AVISO velocity field (with a spatial resolution of 1/4°), a numerical calculation of the marker trajectories was carried out in reverse time over a period of 180 days.

We selected the two-dimensional AVISO altimetry velocity field. This field has been actively used recently to model the transfer pathways of radioactive contamination from the Fukushima nuclear power plant [48] and in the search and identification of places favorable for fishing [50]. The passivity of markers means that they are advected by the velocity field, i.e., as if frozen into it. Passive markers, Lagrangian particles, tracers—these are all synonyms.

Lagrangian trajectories were calculated by solving advection equations:

$$\frac{d\lambda}{dt} = u(\lambda, \varphi, t), \quad \frac{d\varphi}{dt} = v(\lambda, \varphi, t), \quad (1)$$

where  $u$  and  $v$  are angular zonal and meridional components of the AVISO velocity field, and  $\varphi$  and  $\lambda$  are latitude and longitude, respectively. Angular velocities are used to simplify the equations of motion on a sphere. Velocity values inside the cells of the space–time grid were estimated using bicubic interpolation in space and interpolation by Lagrange polynomials of the third degree in time. The simulations of Lagrangian trajectories include the integration of Equation (1) using the fourth-order Runge–Kutta scheme with a constant time step of 0.001 days [47].

### 3. Results

This pattern of possible Amazon River water spread in the tropical Atlantic that has been discussed many times in the literature cited above, along with the satellite maps of surface salinity, was confirmed by altimetry satellite data on the days of our measurements. Figure 3 shows a map of the absolute dynamic topography of the tropical Northwest Atlantic at the time of our measurements in the area where our CTD section intersected the Amazon River water plume (end of January—beginning of February, 2024).

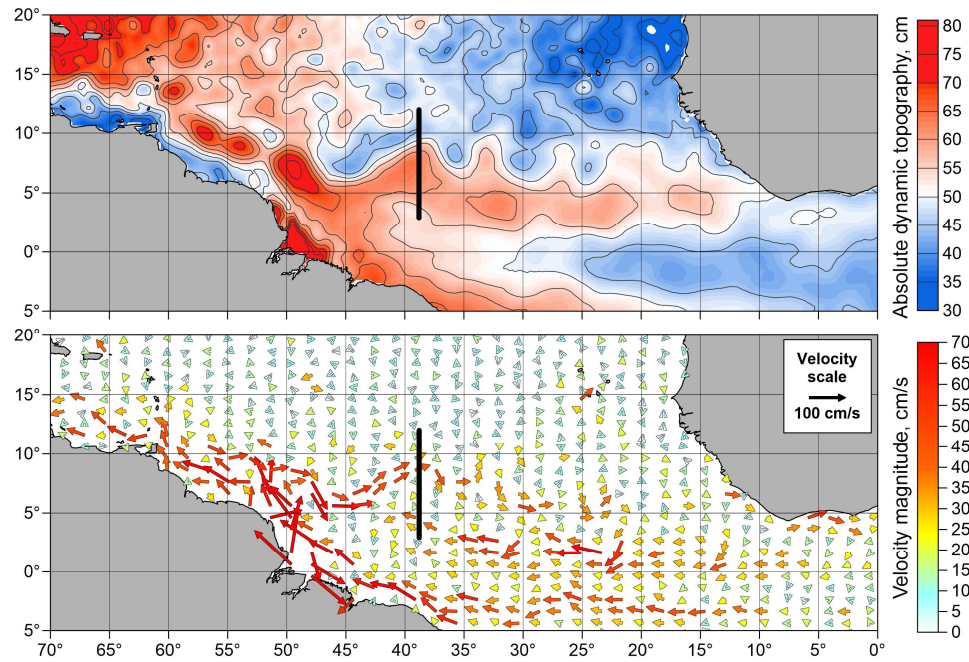


**Figure 3.** Absolute dynamic topography (ADT) of the tropical West Atlantic on 1 February 2024 (**top panel**). Geostrophic currents calculated from the ADT data (**bottom panel**). The black line shows the location of our section from 3° to 12° N. Arrows show velocity vectors. The scale of velocity vectors is shown in the inset.

The vessel performed a meridional section from 3° to 12° N and crossed the North Equatorial Countercurrent (NECC) in the latitudinal range between 7°30' N and 10°00' N. The zonal component of the currents based on the SADCP onboard profiler data is shown in Figure 4. Maximum velocities in the surface layer in the region of the NECC reached 67 cm/s at 9° N. The penetration depth of the NECC was about 200 m.

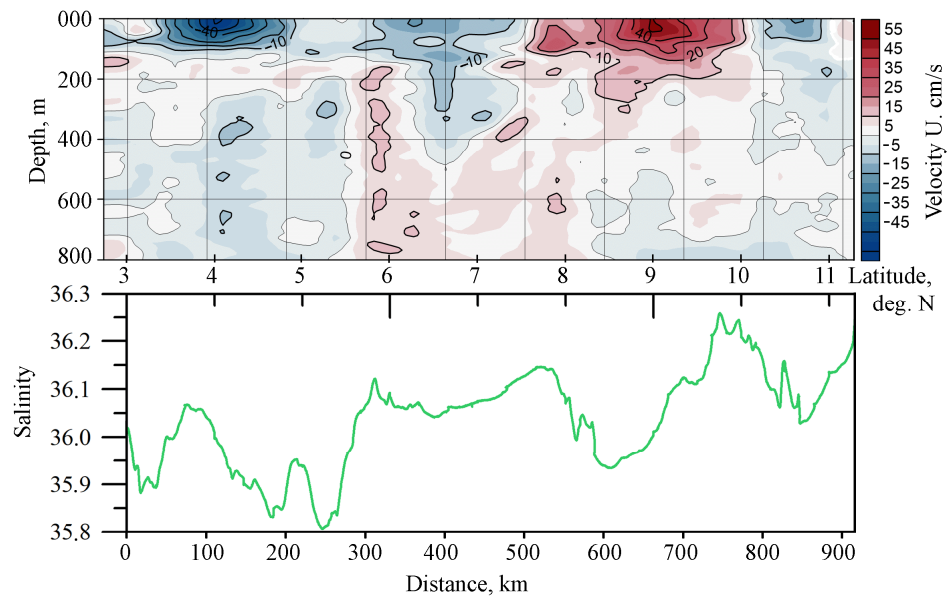


**Figure 4.** Zonal component of the Northern Equatorial Current and other currents over the section from 3°00' N to 12°00' N at 30°48' W (**top panel**). Surface salinity (green line) from flow system data (**bottom panel**). The horizontal scale is the same for both panels.

In this figure, one can also see two cores of high-velocity currents directed to the west at latitudes 4°20' N and 6°30' N. When compared with absolute dynamic topography, these

flows are associated with meandering and rotation to the west of the main current and the transport of desalinated water from the Amazon River plume. Figure 4 also shows surface salinity based on the data of the flow-through system. The low salinities are associated with the westward flow (meandering of the NECC) at  $4^{\circ}00'–5^{\circ}30' N$ . Another salinity minimum was found at  $8^{\circ}30' N$ , which is presumably associated with the eastward flow of the NECC seen in Figure 4 (top panel).

The salinity section based on the data of CTD casts is shown in Figure 5. Since the plume did not spread deeper than 100 m, here, we present a section only in the upper layer of the ocean. The temperature signal was poor because the upper layer is homogenous by temperature to the depths of several tens of meters. The width of the plume was about 170 km derived from the 36 isoline at the surface (from  $4.0^{\circ}$  to  $5.5^{\circ} N$ ), and the depth of desalination was about 90 m. The low salinities below 140 m are related to the general salinity decrease with depth in the equatorial region; it has no relation to the Amazon River water. The salinity difference between the plume in the indicated latitudinal zone and the surrounding waters was 0.25. The plume was mixed, and the mean salinity in the plume was 35.85. The salinity of the water outside the plume was 36.10. This figure also shows the surface salinity based on the data of the flow-through system and turbidity of water, also based on the flow-through data. One of the salinity profiles (at  $5^{\circ}20' N$ ) is shown in the right panel. This graph demonstrates a high vertical gradient of salinity at a depth of  $\sim 100$  m at the bottom of the plume. Here, the salinity difference over an approximately 10 m vertical depth is 0.4. As to the vertical temperature profiles, the upper 100 m layer of the ocean was strongly mixed. The temperature in this layer was close to  $28^{\circ} C$ .

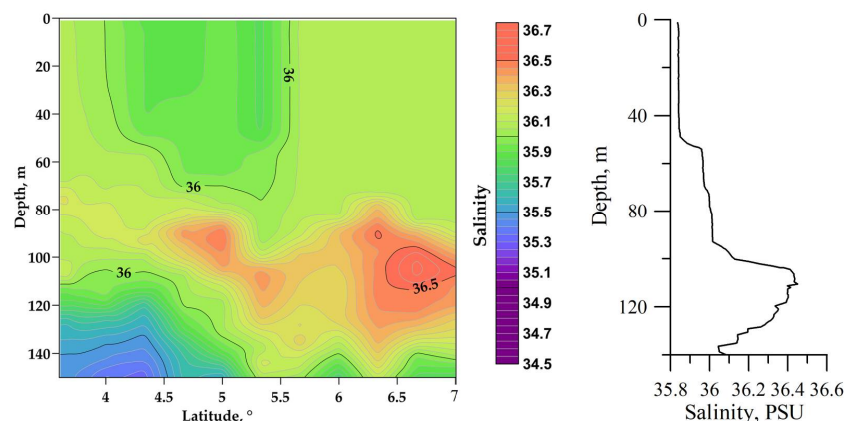


**Figure 5.** Salinity section at the intersection with the plume of desalinated waters at  $38^{\circ}48.0' W$  on 1–2 February 2024 (**left panel**). Salinity profile at the station at latitude  $5^{\circ}20' N$  (**right panel**).

It was reported in [14] that the depth of the plume on the outer edge of the Brazilian shelf northwest of the mouth of the Amazon River was estimated at 15 m, and salinity was about 30 at the outer boundary of the plume. When spreading into the ocean, the depth of mixing due to storms increased to 110 m, and the difference in salinity compared to the background was not more than 0.5. The salinity section normal to the coast of Brazil in [14] shows that already at a distance of 220 km from the coast, desalination reaches depths of 80–90 m, and desalination at the surface is 36.2 compared to the background 36.7.

Continuous recording of salinity near the surface by the vessel's flow-through system shows the presence of two salinity minima: zone I, from  $\sim 4.6^{\circ}$  to  $4.8^{\circ} N$ , and zone II, from  $\sim 5.2^{\circ}$  to  $5.3^{\circ} N$ . One can see that two turbidity maxima coincide with the salinity minima, which confirms the presence of river water in the plume (Figure 6). The turbidity of the waters in this region is very low because most of the suspended matter from the river descended to the deeper layers of the ocean.

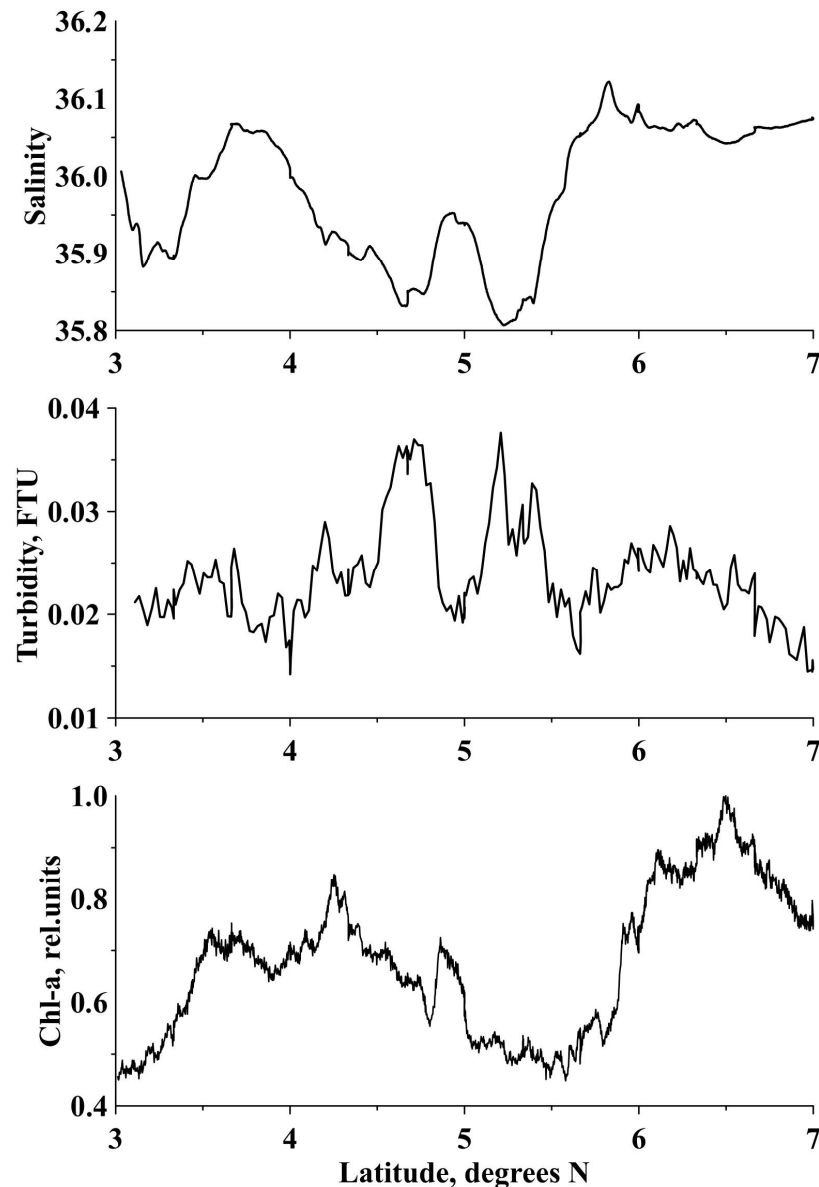


**Figure 6.** Graphs of variations in salinity, turbidity, and chlorophyll-a as recorded by the vessel's flow-through system.

An important additional factor is that these turbidity maxima were not significantly correlated at the 95% significance level with the changes in the intensity of chlorophyll-a fluorescence (Figure 6), which indicates that the development of phytoplankton cells did not influence the results of our measurements at the time of the experiment. In other words, increased turbidity is not associated with increased number of living phytoplankton cells but may be associated with either increased number of dead phytoplankton cells or increased amount of suspended minerals. The available experimental data are insufficient to separate these two possible cases.

Additional confirmation of the relation between remote desalinated seawater with specific river discharges can be provided by Lagrangian modeling in the field of model currents or currents calculated using AVISO data [51]. Figure 7 shows fragments of the propagation of two spots of passive markers back in time to the line 3° N, 47–51° W. The initial positions of the spots were selected at points and at times when, according to the measurements, waters with low salinity were detected. The first spot was launched on 2 February 2024, and the second spot on 4 February 2024 from segment-2. The initial positions of the spots are shown in Figure 7 in black. In both cases, seeded markers

propagate back in time within a compact structure in the North Equatorial Countercurrent (NECC) and North Brazil Current (NBC). However, the propagation trajectories of the spots under consideration are different, which is associated with the high variability of circulation in the study region, which is determined by meandering of the NECC jet.

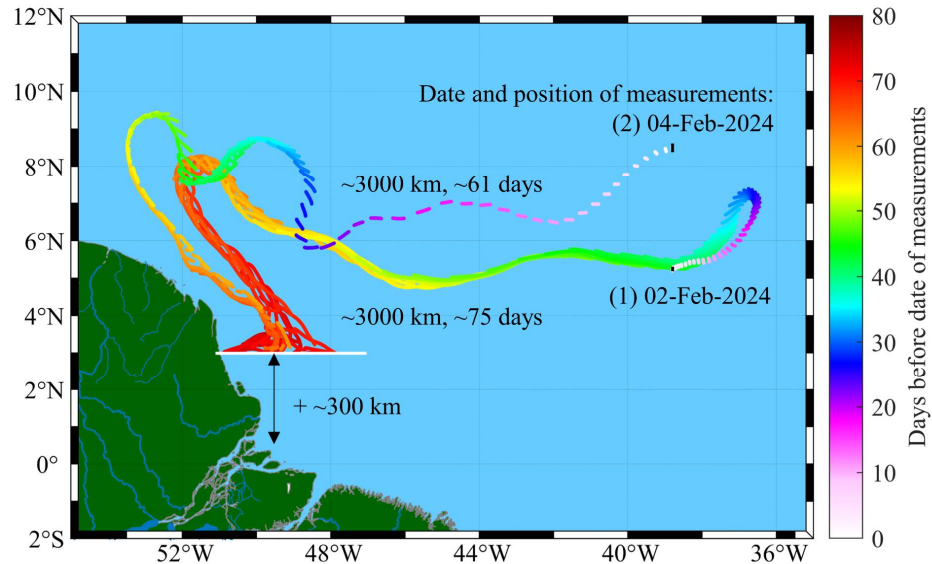


**Figure 7.** Composition of daily traces of trajectories of passive markers simulating Amazon River waters, selected in the segments with the minimum measured salinities ( $5^{\circ}12.0' - 5^{\circ}15.6' \text{ N}$ ,  $38^{\circ}48' \text{ W}$ , 2 February 2024 and  $8^{\circ}27' - 8^{\circ}33' \text{ N}$ ,  $38^{\circ}48' \text{ W}$ , 4 February 2024) over the section. The marker trajectories were calculated back in time over 180 days based on the AVISO velocity field. The initial location of the tracers is indicated with the black dots. The line after which trajectories were not calculated is shown with a white color. Color scale of time is given on the right.

The largest number of seeded markers of the first spot covered the pathway from the place of ship measurements to the white line at  $3^{\circ} \text{ N}$ ,  $47 - 51^{\circ} \text{ W}$  (Figure 7) in 75 days with a mean speed of about 46 cm/s, and the second spot traveled 61 days with a mean speed of 58 cm/s. At the same time, the length of the path traveled by the markers is approximately the same and amounted to about 3000 km (to the white line) in both cases. The markers of the first spot quickly traveled from the white line to  $39^{\circ} \text{ W}$ , covering ~2250 km in 29–30 days (mean speed 88 cm/s). And then, for 40–45 days, they were involved in anticyclonic circulation in a moving eddy, traveling additional ~750 km. This led to the appearance of a loop-like trajectory in the region of  $\sim 5 - 8^{\circ} \text{ N}$  and  $\sim 36 - 39^{\circ} \text{ W}$ .

Thus, considering the additional distance from the mouth of the Amazon River to the white line, waters originating from the river were introduced into the Atlantic Ocean current system in mid-November 2023 for the first segment, and at the beginning of December for the second segment, during the dry season. The time spent by the markers of the first spot to reach the measurement sites was about 60–65 days, and by the markers of the second spot about 75–80 days. In both cases, the distance traveled was about 3300 km including the distance between the white line and the river mouth.

We applied the velocity measurements to estimate the amount of freshwater that was transported by the plume. The mean velocity of the plume in the 100 m layer was 16 cm/s, which agrees with the results of the Lagrangian analysis based on the AVISO geostrophic velocities (Figure 7). The salinity difference between the plume and surrounding water was  $36.10 - 35.85 = 0.25$ , which was thus, 7 mL of additional freshwater from the Amazon River contained in 1 L of seawater in the plume to make lower salinity, at 35.85. The width of the plume was 170 km, and its mean thickness was 70 m (see Figure 2). Hence, one longitudinal meter of the plume contained approximately  $0.12 \times 10^6 \text{ m}^3$  of freshwater from the Amazon River. We calculated the transport by multiplying it by mean velocity

(0.16 m/s, see Figure 4) and obtained an approximate estimate of 0.02 Sv. Thus, only 0.02 Sv of the 0.2 Sv initial transport of firewater from the Amazon River remains in the plume. We think that 10% of the Amazon River water being present in the mid-Atlantic Ocean at an order of magnitude is a reasonable value.

Our measurements were taken in early February 2024. The Amazon River plume is known to have strong seasonal variability. This is demonstrated in satellite images reported in [14]. We were able to find similar data of the CTD section from the WOCE experiment in the WOD18.

The measurement data from WOD18 were made at the end of April 1996. The salinity section based on these data is shown in Figure 8. The section ran along the meridian  $35^{\circ}$  W. The distance between stations was greater than ours (approximately 30 miles). The Amazon River plume turned out to be more desalinated. The width of the plume was greater (more than 450 km, from  $<1.5^{\circ}$  to  $5.8^{\circ}$  N) than during our measurements. The depth of desalination was much shallower (40 m).

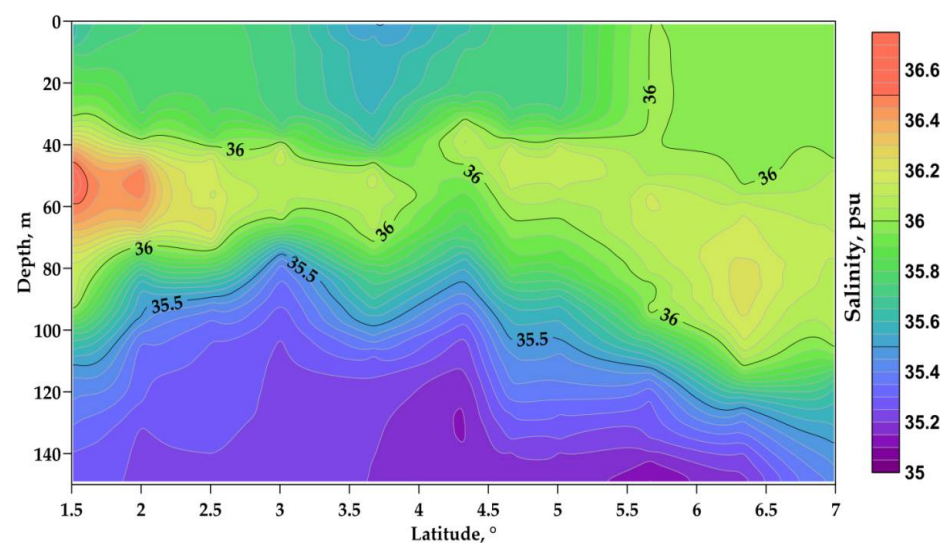


**Figure 8.** Salinity section when crossing a plume of desalinated waters at  $35^{\circ}00'$  W on 27–29 April 1996.

Another set of data from the WOD18 was based on measurements in February 1993. These data showed that the width of the jet was at least 400 km and the depth of desalination was about 60 m, but the jet was displaced to the south compared to our measurements in 2024 (Figure 9).

Such month-to-month variability of the jet reflects the intra-annual variability of water discharge from the Amazon River and plume propagation in the ocean, which was observed from satellite data and described in [14]. The maximum freshening of the plume at longitude of about  $35^{\circ}$  W occurs in August–October. It is associated with a time lag from the maximum Amazon River discharge in June [2]. This can be seen in the satellite images of surface salinity (Figure 10) in February and September for three years. At longitude  $35^{\circ}$  W in September, the plume's latitudinal position is in the range of  $\sim 6$ – $8^{\circ}$  N.

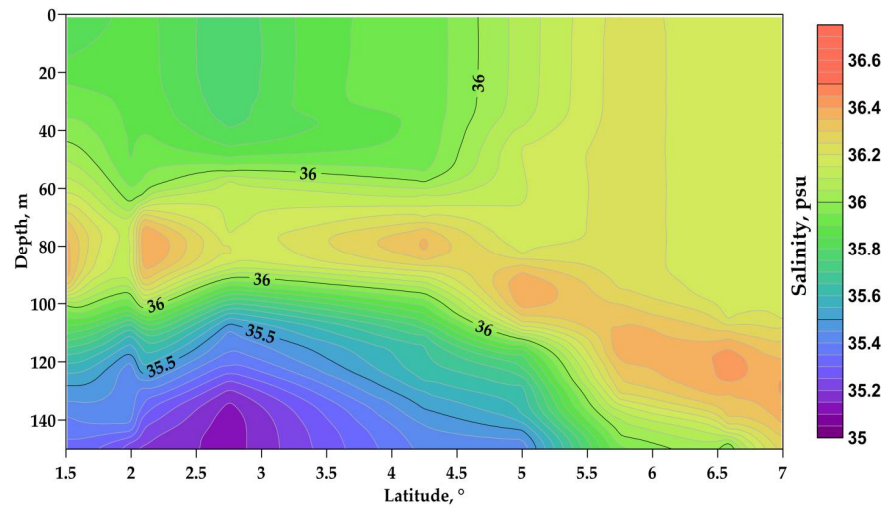


**Figure 9.** Salinity section when crossing a plume of desalinated waters at 35°00' W on 4–5 February 1993.

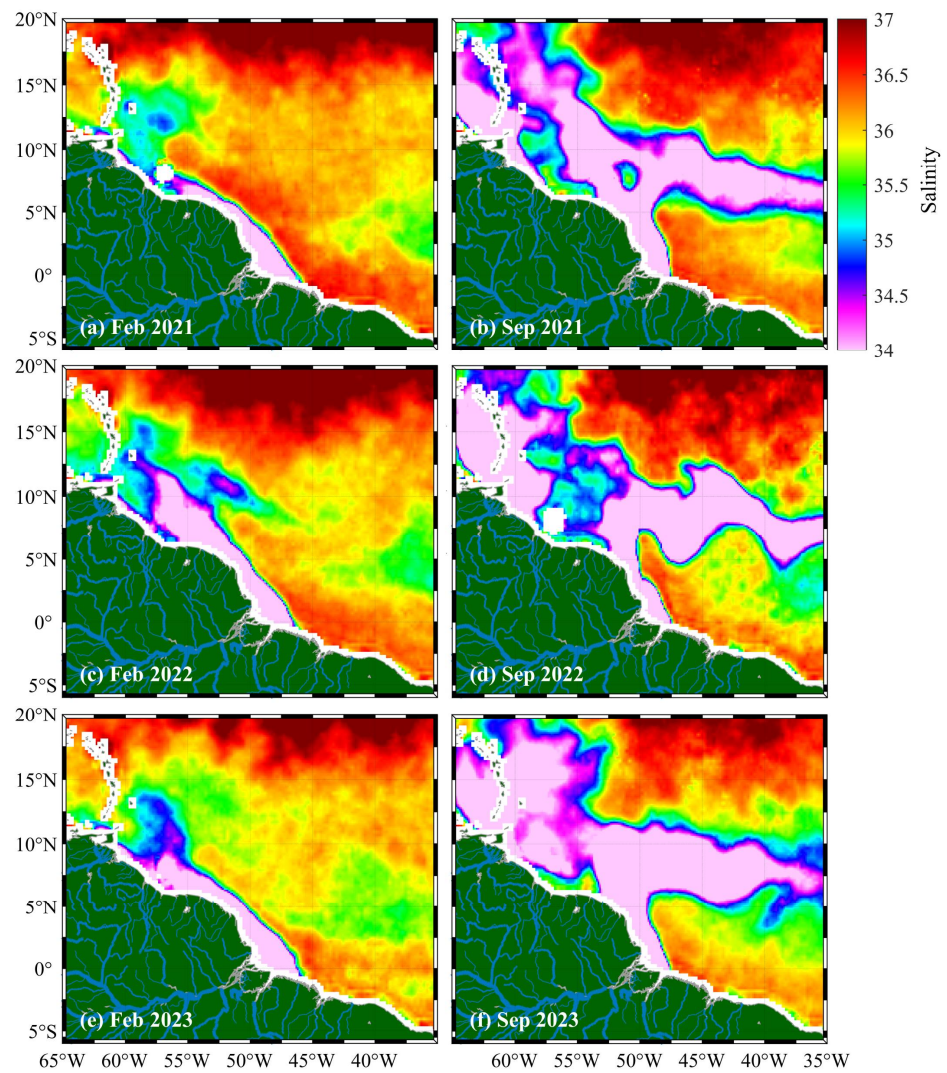


**Figure 10.** Variations in the surface salinity of the Amazon River plume based on the SMAP satellite data in February and September 2021–2023 [18], which is similar to [14] but updated.

We selected several sections in September based on WOD18 data. Not all sections completely covered the plume jet. In September 1986, the section completely crossed the

stream. It turned out that the jet was wider (about 400 km) than during our measurements. Salinity on the surface (34.8) was significantly lower than in the background (36.0). The plume turned out to be shallower, only 40 m (Figure 11). Individual stations with low salinity on the surface in September were carried out in different years. In general, low salinities at the surface were detected during the period of maximum jet development (September) based on the satellite data.

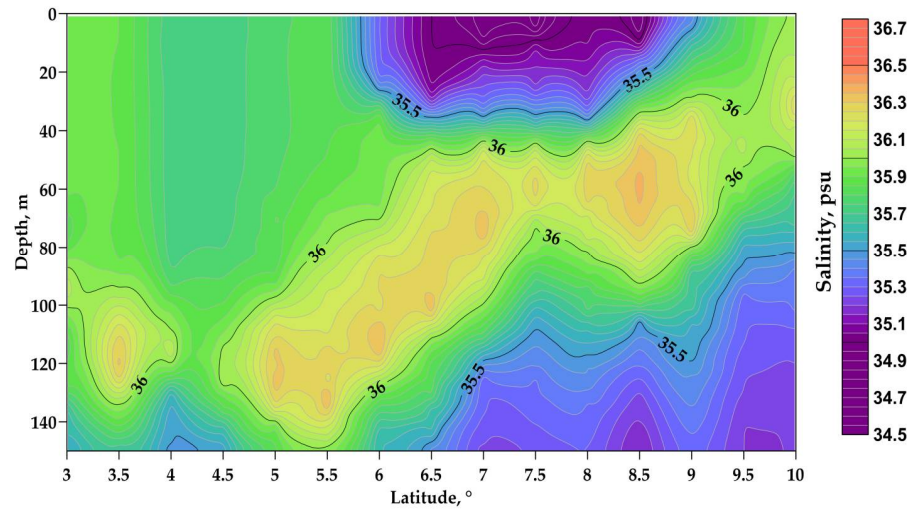


**Figure 11.** Salinity section when crossing a plume of desalinated waters at 34°00' W on 3–5 September 1986.

Individual CTD measurements sometimes reveal surface salinities lower than 33. The deep distribution of salinity in the plume shows that despite a decrease in surface salinity in September, the plume of desalinated waters is much shallower than in February (Figures 11 and 12). A deeper plume core with less freshening can also be detected. Such a core reaches depths of 100 m (Figure 12). Deep penetration of the cores depends on mixing during storms. We think that these two plumes are of different ages and accordingly passed different distances to arrive at the location of measurements.

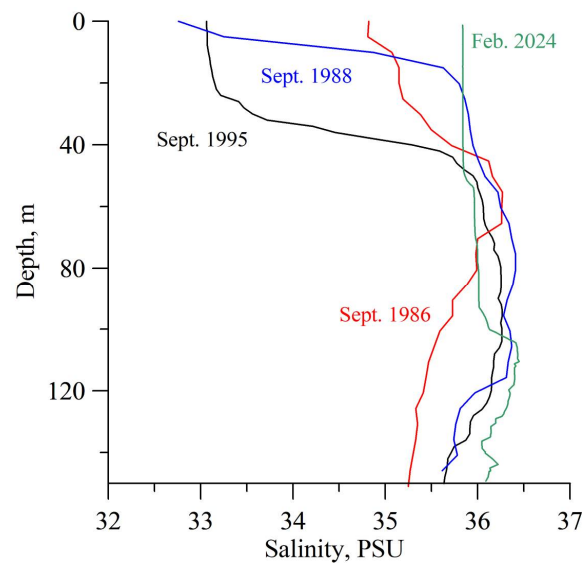


**Figure 12.** Vertical distributions of salinity in September during the period of minimum salinity on the surface in different years in comparison with our data in February 2024.

#### 4. Discussion

The Amazon River discharges large amounts of freshwater into the ocean. This water gradually mixes with the surrounding seawater and spreads to the Atlantic, transported by the North Brazil Current and later by the North Equatorial Countercurrent. As the plume spreads to the ocean, the storms mix the upper layer and low salinity water descends from the surface. At the same time, water at the surface becomes less saline. Our section in February 2024 followed along  $38^{\circ}48' W$ , whereas the Amazon River delta is at  $50^{\circ} W$ . Thus, the direct distance from the Amazon River delta to the region of our measurements exceeded 1200 km. Actually, the distance of freshwater travel was much longer, because first, the plume spread to the northwest following the coastline and only later turned to the east. During propagation, the water can be entrained into mesoscale eddies, which extend the traveled distance.

We applied a Lagrangian analysis to distinguish the pathways of Amazon River water back in time. The revealed pathways generally agree with previous studies of Amazon River freshwater spread [6,9,24,26,32]. It is known from the literature that the amount of freshwater discharge from the Amazon River is subjected to strong seasonal variations [6,13]. This causes seasonal pulses in the spread of the Amazon River plume in the ocean [3,13,15], which is clearly seen on satellite images of surface salinity. The plume is best pronounced in the satellite images of surface salinity in August–December, which follows the maximum river discharge in June [14]. Our estimate of the freshwater flow at  $38^{\circ}48' W$  indicates that 1/10 of the Amazon River discharge at an order of magnitude (0.02 Sv) reaches the region of our measurements. During the propagation the NECC stream meanders and turns back to the west. The percentage of freshwater in the plume was possible to estimate because our approach included velocity measurements using a shipborne SADCP. We also used the historical data from the WOD18 to compare the plume in February with the measurements in other months.

It follows from a comparison of CTD sections made in April, September, and February (Figures 5, 8, 9 and 11) that in September, the plume is located further north than in February and April. One of the causes of the more southern location of the plume after the period of maximum freshening may be associated with the separation of waters from the NECC current due to a series of anticyclonic eddies in the region of  $40$ – $30^{\circ} W$ , arising between the NECC and sNEC, which is typical for the winter season [31].

Crossing of the plume in February shows a greater depth of desalination penetration and higher salinities in the plume than in September. The estimate of travel time from the river's delta to the study site is about 2.0–2.5 months. The plume is best pronounced in September because it consists of water that left the delta region in June during maximum flooding. The water that was recorded in February left the delta region approximately in December, the driest season. Our estimates based on Lagrangian modeling also indicate a travel time on the order of two months.

It is important that both spots of passive markers in Lagrangian modeling based on the AVISO velocity field quite compactly cover the entire distance from the mouth of the Amazon River to the measurement sites without deformations following the formation of the S-shaped folds characteristic of large-scale advection [48]. Such compact advection of spots is associated with the advection of markers, mainly by the main currents of the region.

In addition, we estimated that the plume measured in segment-1 on 2 February 2024 traveled a greater distance from the zone of direct influence of the Amazon River due to additional entrainment into the anticyclonic circulation separated from the NECC current and could also be subject to greater influence of storms and mixing with the surrounding ocean waters. Due to this, there was a greater deepening of the desalinated layer and, hence, an increase in salinity on the surface and throughout the plume layer.

Let us estimate the coefficient of cross-isohaline mixing based on our data. We assume stationarity of the mixing process and modify the following formula from [52], who estimated the coefficient of cross-isothermal mixing in the Romanche Fracture Zone:

$$K_T = \frac{Q^{net}}{A\partial_z\theta'}$$

where  $Q^{net}$  is the pure advective heat flux moving into a volume of water and  $\partial_z\theta$  is the mean vertical temperature gradient over an isothermal surface with area  $A$  and potential temperature  $\theta$ .

We modify this formula for cross-isohaline flux as follows:

$$K_S = \frac{Q^{net}}{A\partial_z S}$$

Approximately 36 kg of salt is additionally transported with one cubic meter of Amazonian freshwater after a period of two months. The mean value is two times smaller because the water was initially fresh. The vertical gradient of salinity in our plume is  $0.5 \text{ kg/m}^3$  over 100 m, which is  $0.005 \text{ kg/m}$ .

Then,  $K_S$  equals

$$K_S = \frac{18 \text{ kg} \times 1 \text{ m}^3}{6.5 \times 10^6 \text{ s} \times 1 \text{ m}^2 \times 0.005 \text{ kg m}^{-1}} = 5.5 \times 10^{-4} \text{ m}^2/\text{s},$$

which is quite reasonable for the ocean under conditions of strong mixing in the upper layer ( $6.5 \times 10^6 \text{ s}$  is approximately 75 days  $\times$  86,400 s). Mixing during storms should be greater. The value given in [34] was five times smaller, and the authors suggested that their estimate exceeded the background value.

We calculated the one-dimensional velocity spectrum of mean velocities in the upper layer (100 m) from the onboard velocity measurements (SADCP data). The spatial sampling was 0.452 km. The spectrum generally decays with increasing wavenumber, but there are two peaks in the high-wavenumber range related to the spatial scales of 3.8 and 5.8 km, which can be associated with small mesoscale rings that induce mixing [32].

Propagation of the Amazon River waters in the Atlantic Ocean has been studied for many years using field measurements [12,14,46], analysis of drifter trajectories [6,9,36], satellite salinity measurements [8,17,40], optically active substances [5,9,17,30,41,42], numerical modeling [17,35,44,45,53], and Lagrangian numerical analysis [54]. We continued this work and applied a comprehensive analysis of the revealed desalination zones in the open ocean to show their relation to the waters of the Amazon River. Each of the methods separately has its own disadvantages and limitations in the context of the reliability of the association of the detected zones with the waters of the Amazon River; however, if we apply a multidisciplinary approach with the simultaneous use and joint interpretation of the data from different methods, it is possible to build an integrated pattern of the transport of river waters. Providing additional confirmation of the adequacy of the Lagrangian estimates for the time of particle transfer is its agreement with the estimates in [6]. The Lagrangian estimates are adequate, which follows from the correspondence of the average speed of motion of passive particles—46 cm/s (~3000 km in 75 days) for section-1 and 57 cm/s (~3000 km in 61 days) for section-2—s values of current velocities in the research region, which vary in the same range (Figures 3 and 4).

The novelty of this work is in the presentation and interpretation of the collected in situ observations in the context of historical observations and studies of the Amazon River plume dynamics. We applied a new approach to use shipborne SADCP measurements of currents and continuous data from the flow-through system of a ship, which makes our analysis different from previous publications. We applied modeling of the motion of freshwater particles back in time before our measurements to show that this freshwater originates from the Amazon River delta.

## 5. Conclusions

We applied a multidisciplinary approach to study the Amazon River plume in the mid-Atlantic. The approach included CTD stations; measurements of velocity using onboard SADC continuous recording of temperature, salinity, chlorophyll-a, and turbidity using a flow-through system on a ship; satellite images; and Lagrangian modeling. Measurements of temperature and salinity in the Amazon River plume far from the river's mouth in the open ocean, with a resolution of 20 miles between stations, revealed the existence of the plume and its detailed structure. The connection with Amazon River discharge was confirmed by the results of flow-through ship measurements of temperature and turbidity. A back-in-time Lagrangian analysis in the AVISO current velocity field showed that the source of freshwater in the measurement region is the Amazon River. Our estimates of freshwater transport across our section ( $38^{\circ}48' W$ ) (0.02 Sv) are one order of magnitude smaller than the mean discharge of the Amazon River (0.2 Sv).

Satellite observations of the plume allow us to study only its surface structure. The measurements allowed us to estimate the width of the Amazon River plume core with salinity less than 36 as 170 km and that of the entire plume as 300–400 km. The desalination depth was from 50 to 100 m. Surface salinity decreased by 0.25 compared to the background (36.1). A comparison with measurements from February of other years showed similar results. A comparison with the measurements in other months, especially in September, when the minimum salinity is usually recorded on the surface based on satellite data, showed that the differences in salinity on the surface with the background salinity beyond the plume amounted to more than 3.

August–October is the period of maximum plume development, which was determined by satellite measurements of surface salinity. The Amazon River discharge reaches its maximum in June, after the rainy season. The spread of the plume to the area of our measurements in February takes about 2.0–2.5 months, during which waters of river origin are transported approximately over 2500–3300 km. The extension of the transport path by approximately 750 km occurs due to additional anticyclonic circulation, which leads to plume motion further to the east and then returns to the southwest. During this time, the plume water mixes with the surrounding waters via storms. Salinity in the plume decreases, and desalinization penetrates to greater depths.

**Author Contributions:** Conceptualization, E.G.M. and P.A.S.; methodology, E.G.M. and M.V.B., software, M.V.B.; validation, D.I.F.; formal analysis, E.G.M. and P.A.S.; data curation, D.I.F. and P.A.S.; writing—original draft preparation, E.G.M., P.A.S. and M.V.B.; writing—review and editing, E.G.M.; funding acquisition, E.G.M. All authors have read and agreed to the published version of the manuscript.

**Funding:** This work was supported by the State Assignment of the Shirshov Institute of Oceanology (FMWE-2024-0016, ship measurements) and the Russian Science Foundation grant 21-77-20004 (analysis of measurement data), as well as by the State Assignments of the Pacific Oceanological Institute FEB RAS No. 124022100080-0 (satellite and flow-through system data) and No. 124022100072-5 (Lagrangian analysis).

**Institutional Review Board Statement:** Not applicable.

**Informed Consent Statement:** Not applicable.

**Data Availability Statement:** If you need to obtain the experimental information and data presented in this paper, please contact the author.

**Acknowledgments:** The authors thank the crew of R/V Akademik Mstislav Keldysh for the assistance in our scientific research.

**Conflicts of Interest:** The authors declare no conflicts of interest.

## References

1. Giffard, P.; Llovel, W.; Jouanno, J.; Morvan, G.; Decharme, D. Contribution of the Amazon River discharge to regional sea level in the tropical Atlantic Ocean. *Water* **2019**, *11*, 2348. [CrossRef]
2. Dai, A.; Trenberth, K.E. Estimates of freshwater discharge from continents: Latitudinal and seasonal variations. *J. Hydrometeorol.* **2002**, *3*, 660–687. [CrossRef]
3. Liang, Y.-C.; Lo, M.-H.; Lan, C.-W.; Seo, H.; Ummenhofer, C.C.; Yeager, S.; Wu, R.-J.; Steffen, J.D. Amplified seasonal cycle in hydroclimate over the Amazon river basin and its plume region. *Nat. Commun.* **2020**, *11*, 4390. [CrossRef]
4. Varona, H.L.; Veleda, D.; Silva, M.; Cintra, M.; Araujo, M. Amazon River plume influence on Western Tropical Atlantic dynamic variability. *Dyn. Atmos. Ocean.* **2019**, *85*, 1–15. [CrossRef]
5. Jo, Y.-H.; Yan, X.-H.; Dzwonkowski, B.; Liu, W.T. A study of the freshwater discharge from the Amazon River into the tropical Atlantic using multi-sensor data. *Geophys. Res. Lett.* **2005**, *32*, L02605. [CrossRef]
6. Coles, V.J.; Brooks, M.T.; Hopkins, J.; Stukel, M.R.; Yager, P.L.; Hood, R.R. The pathways and properties of the Amazon River plume in the tropical North Atlantic Ocean. *J. Geophys. Res. Ocean.* **2013**, *118*, 6894–6913. [CrossRef]
7. Fofonoff, N.P.; Millard, R.C. *Algorithms for Computation of Fundamental Properties of Seawater*; UNESCO Technical Papers in Marine Science; UNESCO: Paris, France, 1983; p. 44.
8. Grodsky, S.A.; Reverdin, G.; Carton, J.A.; Coles, V.J. Year-to-year salinity changes in the Amazon plume: Contrasting 2011 and 2012 Aquarius/SACD and SMOS satellite data. *Remote Sens. Environ.* **2014**, *140*, 14–22. [CrossRef]
9. Hu, C.; Montgomery, E.T.; Schmitt, R.W. The dispersal of the Amazon and Orinoco River water in the tropical Atlantic and Caribbean Sea: Observation from space and S-PALACE floats. *Deep Sea Res. II* **2004**, *51*, 1151–1171. [CrossRef]
10. Muller-Karger, F.E.; McClain, C.R.; Richardson, P.L. The dispersal of the Amazon's water. *Nature* **1988**, *333*, 56–58. [CrossRef]
11. Zeng, N.; Yoon, J.-H.; Marengo, J.A.; Subramaniam, A.; Nobre, C.A.; Mariotti, A.; Neelin, J.D. Causes and impacts of the 2005 Amazon drought. *Environ. Res. Lett.* **2008**, *3*, 014002. [CrossRef]
12. Lentz, S.J.; Limeburner, R. The Amazon River Plume during AMASSEDs: Spatial characteristics and salinity variability. *J. Geophys. Res.* **1995**, *100*, 2355. [CrossRef]
13. Smith, W.O., Jr.; DeMaster, D.J. Phytoplankton biomass and productivity in the Amazon River plume: Correlation with seasonal river discharge. *Cont. Shelf Res.* **1996**, *6*, 227–244. [CrossRef]
14. Morozov, E.G.; Zavialov, P.O.; Zamshin, V.V.; Moller, O.O., Jr.; Frey, D.I.; Zuev, O.A.; Seliverstova, A.M.; Chultsova, A.L.; Bulanov, A.V.; Lipinskaya, N.A.; et al. Mixing zone between the Amazon River plume and open ocean. *Russ. J. Earth Sci.* **2023**, *23*, ES4006. [CrossRef]
15. Cooley, S.R.; Coles, V.J.; Subramaniam, A.; Yager, P.L. Seasonal variations in the Amazon plume-related atmospheric carbon sink. *Glob. Biogeochem. Cycles* **2007**, *21*, GB3014. [CrossRef]
16. Gouveia, N.A.; Gherardi, D.F.M.; Aragão, L.E.O.C. The role of the Amazon River plume on the intensification of the hydrological cycle. *Geophys. Res. Lett.* **2019**, *46*, 12221–12229. [CrossRef]
17. Korosov, A.; Counillon, F.; Johannessen, J.A. Monitoring the spreading of the Amazon freshwater plume by MODIS, SMOS, Aquarius, and TOPAZ. *J. Geophys. Res.* **2015**, *120*, 268–283. [CrossRef]
18. Meissner, T.; Wentz, F.; Manaster, A.; Lindsley, R.; Brewer, M.; Densberger, M. NASA/RSS SMAP Salinity: Version 5.0 Validated Release. RSS Technical Report 82219. Remote Sensing Systems: Santa Rosa, CA, USA, 2022; p. 64. Available online: [https://data.remss.com/smap/SSS/V05.0/documents/SMAP\\_NASA\\_RSS\\_Salinity\\_Release\\_V5.0.pdf](https://data.remss.com/smap/SSS/V05.0/documents/SMAP_NASA_RSS_Salinity_Release_V5.0.pdf) (accessed on 10 May 2024).
19. Muller-Karger, F.E.; McClain, C.R.; Fisher, T.R.; Esaias, W.E.; Varela, R. Pigment distribution in the Caribbean Sea: Observations from space. *Prog. Oceanogr.* **1989**, *23*, 23–64. [CrossRef]
20. Hochman, H.T.; Muller-Krager, F.E.; Walsh, J.J. Interpretation of the coastal zone color scanner signature of the Orinoco River plume. *J. Geophys. Res.* **1994**, *99*, 7443–7455. [CrossRef]
21. Fratantoni, D.M.; Glickson, D.A. North Brazil Current Ring generation and evolution observed with SeaWiFS. *J. Phys. Oceanogr.* **2002**, *32*, 1058–1074. [CrossRef]
22. Johns, E.M.; Muhling, B.A.; Perez, R.C.; Muller-Karger, F.E.; Melo, N.; Smith, R.H.; Lamkin, J.T.; Gerard, T.L.; Malca, E. Amazon River water in the northeastern Caribbean Sea and its effect on larval reef fish assemblages during April 2009. *Fish. Oceanogr.* **2014**, *23*, 472–494. [CrossRef]
23. Ou, H.W.; DeRuijter, W.P. Separation of an inertial boundary current from a curved coastline. *J. Phys. Oceanogr.* **1986**, *16*, 280–289. [CrossRef]
24. Fratantoni, D.M.; Johns, W.E.; Townsend, T.L. Rings of the North Brazil Current: Their structure and behavior inferred from observations and a numerical simulation. *J. Geophys. Res.* **1995**, *100*, 10633–10654. [CrossRef]
25. Johns, W.E.; Beardsley, R.C.; Candela, J.; Limeburner, R.; Castro, B. Annual cycle and variability of the North Brazil Current. *J. Phys. Oceanogr.* **1998**, *28*, 103–128. [CrossRef]
26. Fratantoni, D.M.; Richardson, P.L. The evolution and demise of North Brazil Current rings. *J. Phys. Oceanogr.* **2006**, *36*, 1241–1264. [CrossRef]
27. Garzoli, S.L.; Field, A.; Yao, Q. *North Brazil Current Rings and the Variability in the Latitude of Retroreflection*; Goni, G.J., Malanotte-Rizzoli, P., Eds.; Elsevier Oceanography Series; Elsevier: Amsterdam, The Netherlands, 2003; Volume 68, pp. 357–373. [CrossRef]
28. Hellweger, F.; Gordon, A. Tracing Amazon River water into the Caribbean Sea. *J. Mar. Res.* **2002**, *60*, 537–549. [CrossRef]

29. Vallès-Casanova, I.; Fraile-Nuez, E.; Martín-Rey, M.; van Sebille, E.; Cabré, A.; Olivé-Abelló, A.; Pelegrí, J.L. Water mass transports and pathways in the North Brazil-Equatorial Undercurrent retroflection. *J. Geophys. Res.* **2022**, *127*, e2021JC018150. [[CrossRef](#)]
30. Salisbury, J.; Vandemark, D.; Campbell, J.; Hunt, C.; Wisser, D.; Reul, N.; Chapron, B. Spatial and temporal coherence between Amazon River discharge, salinity, and light absorption by colored organic carbon in western tropical Atlantic surface waters. *J. Geophys. Res.* **2011**, *116*, C00H02. [[CrossRef](#)]
31. Dimoune, D.M.; Birol, F.; Hernandez, F.; Léger, F.; Araujo, M. Revisiting the tropical Atlantic western boundary circulation from a 25-year time series of satellite altimetry data. *Ocean Sci.* **2023**, *19*, 251–268. [[CrossRef](#)]
32. Aguedjou, H.M.A.; Chaigneau, A.; Dadou, I.; Morel, Y.; Pegliasco, C.; Da-Allada, C.Y.; Baloitcha, E. What can we learn from observed temperature and salinity isopycnal anomalies at eddy generation sites? Application in the tropical Atlantic Ocean. *J. Geophys. Res.* **2021**, *126*, e2021JC017630. [[CrossRef](#)]
33. Philander, S. *Atlantic Ocean Equatorial Currents*; Princeton University Academic Press: Princeton, NJ, USA, 2001; pp. 188–191. [[CrossRef](#)]
34. Romanova, V.; Köhl, A.; Stammer, D. Seasonal cycle of near-surface freshwater budget in the western tropical Atlantic. *J. Geophys. Res.* **2011**, *116*, C07009. [[CrossRef](#)]
35. Ferry, N.; Reverdin, G. Sea surface salinity interannual variability in the western tropical Atlantic: An ocean general circulation model study. *J. Geophys. Res.* **2004**, *109*, C05026. [[CrossRef](#)]
36. Limeburner, R.; Beardsley, R.C.; Soares, I.D.; Lentz, S.J.; Candela, J. Lagrangian flow observations of the Amazon River discharge into the North Atlantic. *J. Geophys. Res.* **1995**, *100*, 2401–2415. [[CrossRef](#)]
37. Deppenmeier, A.-L.; Haarsma, R.J.; LeSager, P.; Hazeleger, W. The effect of vertical ocean mixing on the tropical Atlantic in a coupled global climate model. *Clim. Dyn.* **2020**, *54*, 5089–5109. [[CrossRef](#)]
38. Castellanos, P.; Pelegrí, J.L.; Campos, E.J.D.; Rosell-Fieschi, M.; Gasser, M. Response of the surface tropical Atlantic Ocean to wind forcing. *Prog. Oceanogr.* **2015**, *134*, 271–292. [[CrossRef](#)]
39. Yu, L. A global relationship between the ocean water cycle and near-surface salinity. *J. Geophys. Res.* **2011**, *116*. [[CrossRef](#)]
40. Tzortzi, E.; Josey, S.A.; Srokosz, M.; Gommenginger, C. Tropical Atlantic salinity variability: New insights from SMOS. *Geophys. Res. Lett.* **2013**, *40*, 2143–2147. [[CrossRef](#)]
41. Del Vecchio, R.; Subramaniam, A. Influence of the Amazon River on the surface optical properties of the western tropical North Atlantic Ocean. *J. Geophys. Res.* **2004**, *109*. [[CrossRef](#)]
42. Medeiros, P.M.; Seidel, M.; Ward, N.D.; Carpenter, E.J.; Gomes, H.R.; Niggemann, J.; Krusche, A.V.; Richey, J.E.; Yager, P.L.; Dittmar, T. Fate of the Amazon River dissolved organic matter in the tropical Atlantic Ocean. *Glob. Biogeochem. Cycles* **2015**, *29*, 677–690. [[CrossRef](#)]
43. Gévaudan, M.; Durand, F.; Jouanno, J. Influence of the Amazon-Orinoco discharge interannual variability on the western tropical Atlantic salinity and temperature. *J. Geophys. Res.* **2022**, *127*, e2022JC018495. [[CrossRef](#)]
44. Awo, F.M.; Alory, G.; Da-Allada, C.Y.; Delcroix, T.; Jouanno, J.; Kestenare, E.; Baloitcha, E. Sea surface salinity signature of the tropical Atlantic interannual climatic modes. *J. Geophys. Res.* **2018**, *123*, 7420–7437. [[CrossRef](#)]
45. Nikiema, O.; Devenon, J.-L.; Baklouti, M. Numerical modeling of the Amazon River plume. *Cont. Shelf Res.* **2007**, *27*, 873–899. [[CrossRef](#)]
46. Lefèvre, N.; Tyaquicã, P.; Veleza, D.; Perruche, C.; Van Gennip, S.J. Amazon River propagation evidenced by a CO<sub>2</sub> decrease at 8 N, 38 W in September 2013. *J. Mar. Syst.* **2020**, *211*, 103419. [[CrossRef](#)]
47. Prants, S.V. Backward-in-time methods to simulate large-scale transport and mixing in the ocean. *Phys. Scr.* **2015**, *90*, 074054. [[CrossRef](#)]
48. Budyansky, M.V.; Udalov, A.A.; Lebedeva, M.A.; Belonenko, T.V. Assessment of pollution of the waters in the South Kuril Fishing Zone of Russia by radioactive waters from the Fukushima-1 NPP based on Lagrangian Modeling. *Dokl. Earth Sci.* **2024**, *515*, 458–467. [[CrossRef](#)]
49. Budyansky, M.V.; Goryachev, V.A.; Kaplunenko, D.D.; Lobanov, V.B.; Prants, S.V.; Sergeev, A.F.; Shlyk, N.V.; Uleysky, M.Y. Role of mesoscale eddies in transport of Fukushima-derived cesium isotopes in the ocean. *Deep Sea Res. I* **2015**, *96*, 15–27. [[CrossRef](#)]
50. Prants, S.V.; Budyansky, M.V.; Uleysky, M.Y.; Kulik, V.V. Lagrangian fronts and saury catch locations in the Northwestern Pacific in 2004–2019. *J. Mar. Syst.* **2021**, *222*, L17203. [[CrossRef](#)]
51. Fayman, P.A.; Salyuk, P.A.; Budyansky, M.V.; Burenin, A.V.; Didov, A.A.; Lipinskaya, N.A.; Ponomarev, V.I.; Udalov, A.A.; Morgunov, Y.N.; Uleysky, M.Y.; et al. Transport of the Tumen River Water to the Far Eastern Marine Reserve (Posyet Bay) Based on in Situ, Satellite Data and Lagrangian Modeling Using ROMS Current Velocity Output. *Mar. Pollut. Bull.* **2023**, *194*, 115414. [[CrossRef](#)] [[PubMed](#)]
52. Ferron, B.; Mercier, H.; Speer, K.; Gargett, A.; Polzin, K. Mixing in the Romanche Fracture Zone. *J. Phys. Oceanogr.* **1998**, *28*, 1929–1945. [[CrossRef](#)]

- 
53. Garzoli, S.L. The Atlantic North equatorial countercurrent: Models and observations. *J. Geophys. Res.* **1992**, *97*, 17931–17946. [[CrossRef](#)]
  54. de Freitas, P.P.; Cirano, M.; Teixeira, C.E.P.; Marta-Almeida, M.; de Brito Borges, F.F.; Guerrero-Martin, C.A.; Costa Gomes, V.J. Pathways of surface oceanic water intrusion into the Amazon Continental Shelf. *Ocean. Dyn.* **2024**, *74*, 321–334. [[CrossRef](#)]

**Disclaimer/Publisher’s Note:** The statements, opinions and data contained in all publications are solely those of the individual author(s) and contributor(s) and not of MDPI and/or the editor(s). MDPI and/or the editor(s) disclaim responsibility for any injury to people or property resulting from any ideas, methods, instructions or products referred to in the content.